

AERODYNAMIC STUDY OF A SMALL-SCALE WIND TURBINE.

E. Barbier^a, P. Bucello^a, S. D'hers^a, P. Mosquera Michaelsen^b, B. Pritz^b, N. Bottini^c and M. Micheloud^c

^a*Centro de Mecánica Computacional, Instituto Tecnológico de Buenos Aires, Av. E. Madero 399, Buenos Aires, Argentina, pbucello@itba.edu.ar, http://www.itba.edu.ar/lab_mecanica_computacional*

^b*Institute of Fluid Machinery, Karlsruhe Institute of Technology, Kaiserstrasse 12 Karlsruhe, Germany, pritz@kit.edu, <http://www.fsm.kit.edu>*

^c*ALP Group, Buenos Aires, Argentina, matias.micheloud@alpgroup.com.ar, <http://www.alpgroup.com.ar>*

Keywords: Computational Fluid Dynamics, Fluid Structure Interaction, Wind Turbine, HAWT.

Abstract.

Wind is becoming a competitive energy source, dragging more and more attention as a renewable, economically viable and *greener* alternative to traditional sources. Large scale wind farms connected to national power grids are today very common in Europe and USA. In the other end of wind power generation spectrum, we find small-scale wind turbines designed and built to be used at isolated spots, such as farms in the Argentinean Patagonia. In these small scale applications, the impossibility to connect to the national power grid adds an additional interest to the use of wind turbines as a source of electric energy.

In the present work an aerodynamic study of a small-scale commercial wind turbine is performed, using simplified theoretical models and 2D and 3D CFD calculations. Turbine power output is estimated and compared with experimental measurements. Pressure distribution over the blades is calculated, in order to perform Fluid Structure Interaction (FSI) analyses. Conclusions and future work are stated.

1 INTRODUCTION

Growing awareness of environmental issues such as global warming, greenhouse effect and air pollution, together with the increasing prices of fossil fuels have boosted the interest in developing renewable and environmentally friendly power sources (Cooper *et al.*, 2010). Wind energy has become a particularly successful one, showing sustained and significant growth (Kaldellis, 2004).

1.1 Small-scale wind turbines.

While most of wind generated electricity is produced by large scale wind turbines (more than 50kW of electrical power), isolated communities with no connectivity to national power grids may use small-scale wind turbines as an alternative to diesel generators. Wind turbines have been used for household electricity generation in conjunction with battery storage over many decades in remote areas. Small-scale wind turbines are categorized as micro (1 kW), mid-range (5 kW) and mini wind turbines (20 kW) (Clausen and Wood, 1999; Ronit *et al.*, 2013). A more detailed description of micro wind turbines can be found in Cooper *et al.* (2010) and Peacock *et al.* (2008).

1.2 Costa-I micro wind turbine.

In the present work the aerodynamic characteristics of **Costa-I** micro wind turbine are analysed. Costa-I wind turbine is a horizontal axis wind turbine (HAWT) designed for domestic use in rural areas, produced and commercialized in Argentina by **ALP Group** (<http://www.alpgroup.com.ar>). Principal features are summarized in Table 1.

Nominal power output	1.1kW @ 10m/s
Power control method	furl control starting at 10m/s
Number of blades	3
Diameter	3.3m
Rotational speed	300rpm
Aerodynamic profile	AH 93-W-145
Installation height	9 - 13m

Table 1: **Costa-I** principal features.

2 AERODYNAMIC STUDY.

Costa-I wind turbine aerodynamic characteristics are analysed using different models. Power output is estimated with the following methods:

1. One-Dimensional Momentum Theory (Betz theory);
2. Blade Element Momentum (BEM) Theory.
3. Direct power calculation using 3D CDF models.

2.1 One-Dimensional Momentum Theory (Betz theory).

A simple model, generally attributed to Betz (Betz, 1994), can be used to determine the power from an ideal turbine rotor, the thrust of the wind on the ideal rotor, and the effect of the rotor operation on the local wind field (Manwell *et al.*, 2009).

This analysis assumes a control volume which is delimited by a stream tube and two cross sections of the latter. The turbine is idealized as a uniform actuator disk creating a pressure discontinuity in the flow (see Fig. 1). The following assumptions are made:

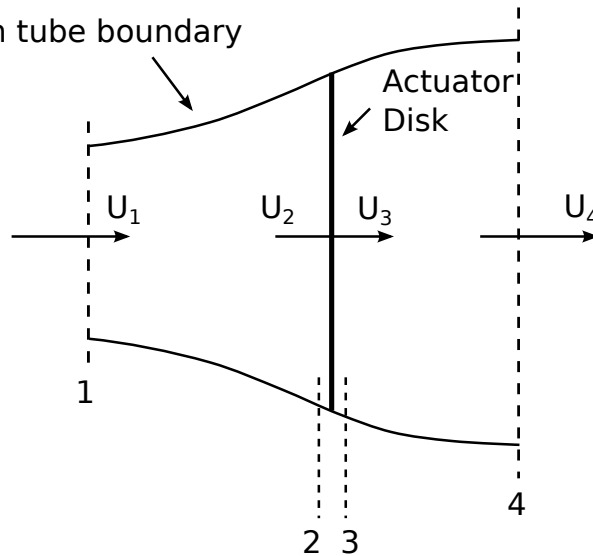


Figure 1: Actuator disk model of a wind turbine.

- the flow is ideal (homogenous, incompressible, frictionless, steady state fluid flow) and rectilinear;
- thrust and flow are uniform across the rotor area;
- non-rotating wake;
- static pressure at the upwind and downwind boundaries is equal to the undisturbed ambient pressure.

Enforcing linear momentum, mass and energy conservation and assuming $U_2 = U_3$, one gets:

$$U_2 = \frac{U_1 + U_4}{2}, \quad (1)$$

i.e., the flow velocity at the rotor plane is the arithmetic mean of the upstream and downstream speeds. The *induction factor* is defined as:

$$a = \frac{U_1 - U_2}{U_1}. \quad (2)$$

Definition (2) and Eq. (1) gives:

$$\begin{aligned} U_2 &= U_1(1 - a), \\ U_4 &= U_1(1 - 2a); \end{aligned} \quad (3)$$

and the power output P of the turbine is:

$$P = \frac{1}{2} \rho A U_1^3 4a(1 - a)^2, \quad (4)$$

where A is the actuator disk area and ρ is the air density. The factor $\frac{1}{2}\rho AU_1^3$ in Eq. (4) is the power carried by the incoming flow. The ratio

$$C_P = \frac{P}{\frac{1}{2}\rho AU_1^3} = 4a(1-a)^2 \quad (5)$$

is called *power coefficient* of the wind turbine rotor, and represents the fraction of the power in the flow that is extracted by the rotor. Although induction factor a is not known, Eq. (4) can be used to derive an upper bound for power output, by finding an optimal value for a so that C_P attains a maximum, as shown in Fig. 2. Maximum power coefficient for an ideal frictionless

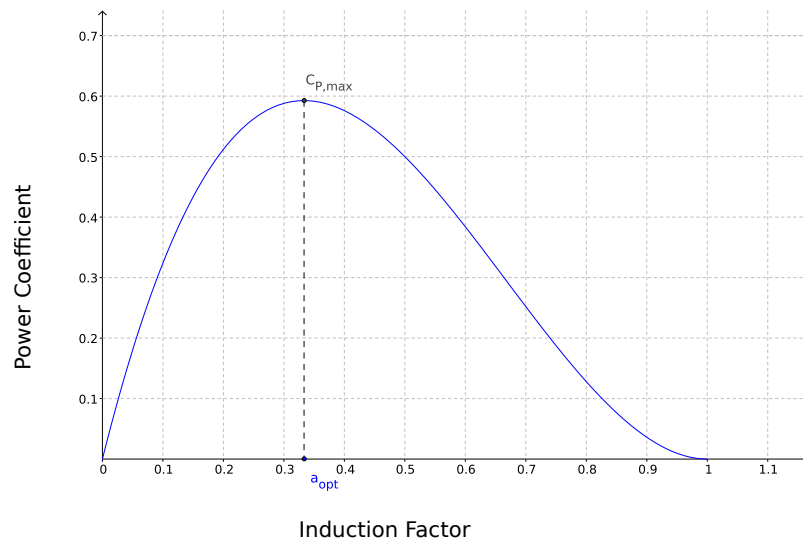


Figure 2: Power Coefficient vs. Induction Factor.

turbine is thus $C_{P,max} = \frac{16}{27} \approx 0.593$. This value is known as *Betz limit*. It should be pointed out that Eq. (4) is not valid for $a \geq 0.5$, as $a = 0.5$ would imply that downstream velocity is zero, and a negative a would imply that the flow reverses direction. For further details, see [Manwell et al. \(2009\)](#). For the **Costa-I** wind turbine parameters, the Betz limit is 3180W.

2.2 Blade Element Momentum (BEM) Theory.

The previous analysis can be modified and integrated with aerofoil theory to produce a more realistic model accounting for:

- angular momentum in the wake;
- non-uniform pressure and turbulence distribution over the swept area;
- aerodynamic drag;
- finite number of blades.

The flow upstream the rotor plane is purely rectilinear, but if the rotor acquires angular momentum through its interaction with the flow, as a consequence of angular momentum conservation, the flow past the rotor must acquire an equal amount of angular momentum, in the opposite direction (i.e., the wake acquires rotational velocity, see [Manwell et al. \(2009\)](#)).

If rotor angular velocity is Ω , and wake angular velocity is ω , the *angular induction factor* a' is defined as:

$$a' = \frac{\omega}{2\Omega}. \quad (6)$$

25/07 The *local speed ratio* λ_r is defined as:

$$\lambda_r = \frac{\Omega r}{U} = \frac{\lambda r}{R}, \quad (7)$$

where $\lambda = \frac{\Omega R}{U}$ is the *tip speed ratio*.

With these definitions, relative flow speed angle φ with respect to the rotation plane at a particular radial position r can be expressed as (see Fig. 3):

$$\tan \varphi = \frac{U(1-a)}{\Omega r(1+a')} = \frac{1-a}{\lambda_r(1+a')} \quad (8)$$

Dividing the rotor in annular sections with radius r and thickness dr , and assuming that pres-

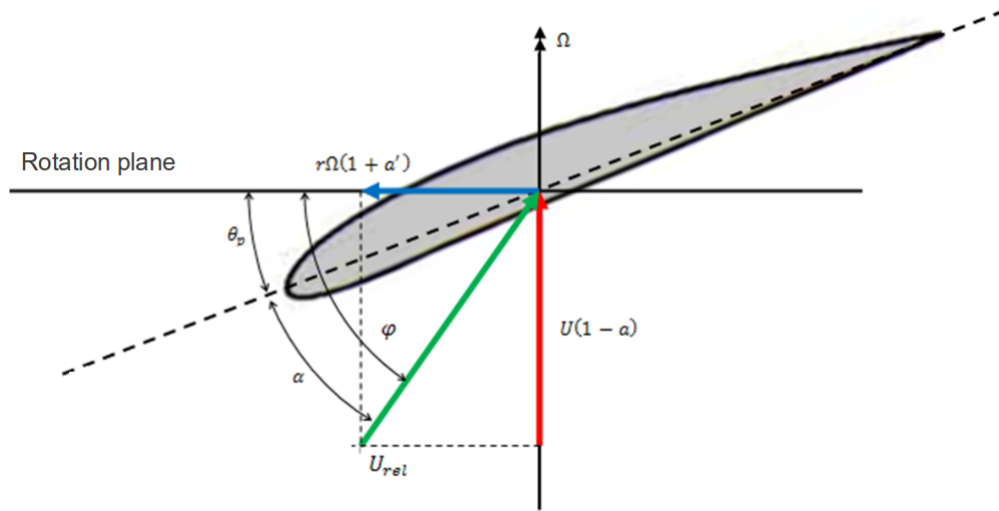


Figure 3: Relative velocity.

sure, wake rotation and induction factors are functions of radius only, rotor power can be calculated as:

$$P = \int_0^R B\Omega \frac{1}{2} \rho U_{rel}^2 (C_l \sin \varphi - C_d \cos \varphi) c r dr, \quad (9)$$

where B is the number of blades, ρ is fluid density, c is chord length, and C_l , C_d are the lift and drag coefficients, respectively.

It can be shown that, if one assumes $C_d = 0$ (see [Manwell et al. \(2009\)](#)),

$$C_l = 4 \sin \varphi \frac{\cos \varphi - \lambda_r \sin \varphi}{\frac{Bc}{2\pi r} (\sin \varphi + \lambda_r \cos \varphi)}. \quad (10)$$

Realizing from Fig. 3 that $\varphi = \alpha + \theta_p$ and recalling from 2D aerofoil theory that C_l is a function of angle of attack α , one can solve Eq. (10) together with $C_l = C_l(\alpha)$ to find local angle of attack

α^* and corresponding lift coefficient C_l^* at radius r . Using the following relations (see [Manwell et al. \(2009\)](#)):

$$\frac{a'}{1+a'} = \frac{Bc}{2\pi r} \frac{C_l}{4 \cos \varphi} \quad (11)$$

$$a = a' \frac{\lambda_r}{\tan \varphi},$$

induction factors can be determined (it should be verified that condition $a < 0.5$ is satisfied), and then Eq. (9) gives rotor power.

A practical implementation of the method just outlined is:

1. divide the rotor blade into strips of finite length Δr ,
2. assume that $c, \theta_p, \alpha, C_l, C_d, a, a'$ are constant within each strip,
3. determine the aforementioned parameters,
4. calculate rotor power.

Power losses due to wingtip effect can be taken into account by multiplying each strip's contribution to total power by Prandtl's correction factor F ([de Vries, 1979](#)):

$$F = \frac{2}{\pi} \cos^{-1} \left[\exp \left(-\frac{\frac{B}{2} \left[1 - \frac{r}{R} \right]}{\frac{r}{R} \sin \varphi} \right) \right]. \quad (12)$$

2.2.1 BEM analysis of Costa-I.

As stated in Table 1 of 1.2, **Costa-I** blades' aerodynamic profile is **AH 93-W-145** ([Althaus, 1996](#)), see Fig. 4.

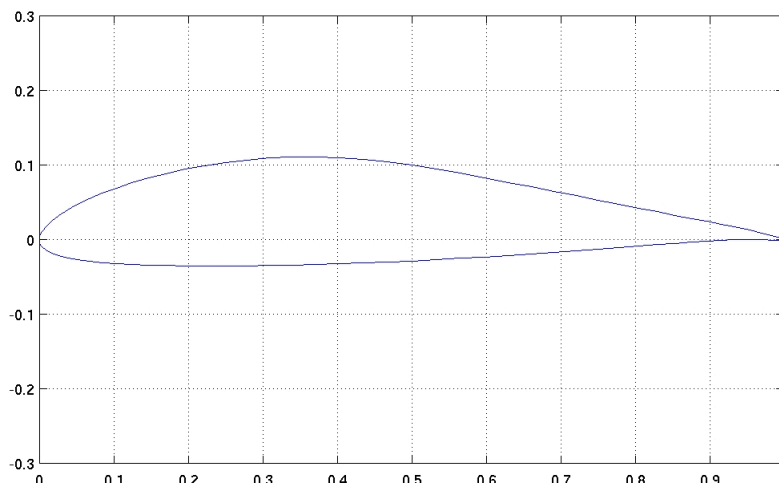


Figure 4: AH 93-W-145 aerofoil.

Lift and drag coefficients for this profile are calculated using 2D CFD models developed both in SPARC and ANSYS-CFX, for angles of attack varying from 0° to 22° . Simulations are performed in conditions of no rugosity, sub-sonic flow and $R_e \approx 1.5 \times 10^6$. Turbulence is coped

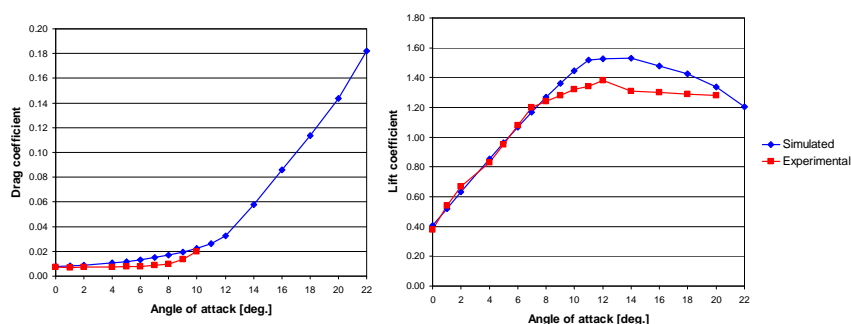
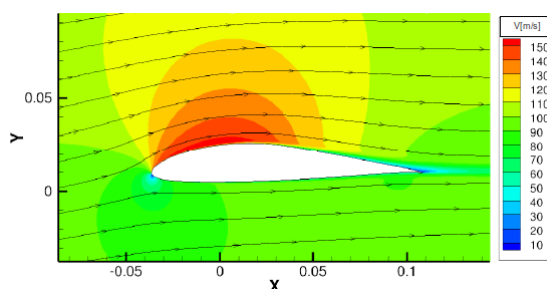
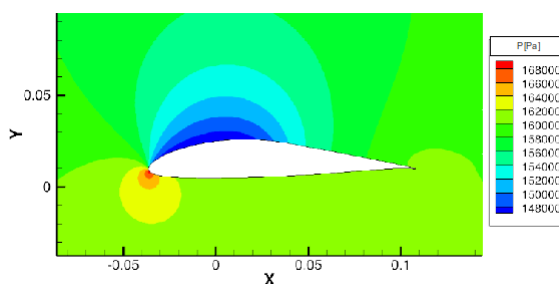


Figure 5: Lift and Drag coefficients.

with the Spalart-Allmaras model (Pletcher et al., 2013). Numerical and experimental results show very good agreement, as can be seen in Fig. 5.

Velocity and pressure distribution for an angle of attack $\alpha = 5^\circ$ are shown in Figs. 6 and 7, respectively.

Figure 6: Velocity distribution, $\alpha = 5^\circ$.Figure 7: Pressure distribution, $\alpha = 5^\circ$.

Using these results and the procedure outlined in 2.2, estimated power output for **Costa-I** wind turbine is 2400W, and corresponding power coefficient is $C_P = 0.447$.

2.3 Direct power calculation using 3D CFD models.

A 3D CFD model developed in ANSYS-CFX is used to predict power output and pressure distribution along the blades. Main features of this model are:

- cyclic symmetry (only 1/3 of the turbine is modelled);
- disturbances due to mounting tower are neglected;

- rotating structured mesh (about 1.5×10^6 cells);
- stationary analysis;
- turbulence modelled using Spalart-Allmaras turbulence model.

Computational domain and boundary conditions can be seen in Fig. 8.

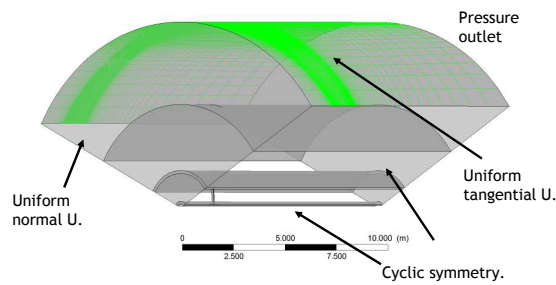


Figure 8: Computational domain and boundary conditions for 3D CFD model.

This model is used to predict power output for wind speed varying from 3m/s to 13m/s, at a rotational speed of 300rpm. At nominal speed of 10m/s, predicted power output is 2350W and $C_P = 0.438$, which is in close agreement with the result of the BEM model.

Field measurements and predicted power output show good agreement, as can be seen in Fig. 9 (estimated power output is affected by a factor of 0.64 accounting for electrical and mechanical losses). Discrepancy between numerical simulation and experimental results for wind speed greater than 8m/s is attributed to the action of furl control. Fig. 10 shows streamlines

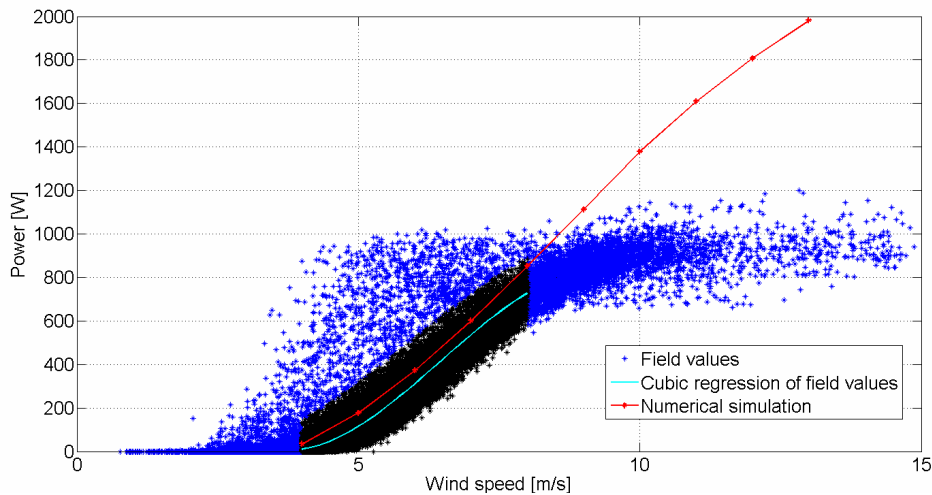


Figure 9: 3D CFD model power prediction and experimental values.

of the flow field, wake rotation can be clearly seen. Velocity field at rotor plane is shown in Fig. 11. Pressure contour plots and streamlines at different sections are shown in Figs. 12 thru 14. This pressure distribution can be used as input data for a fluid structure interaction (FSI) model.

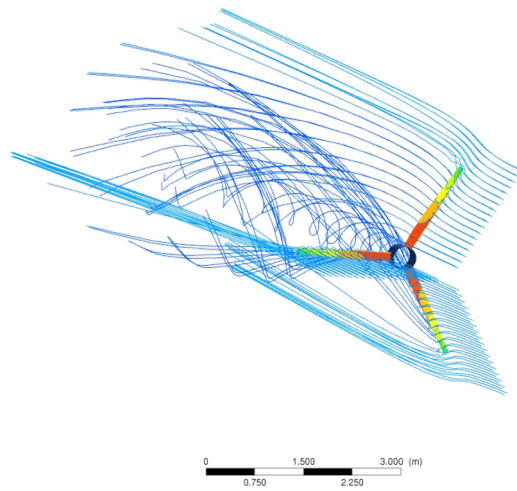


Figure 10: Streamlines.

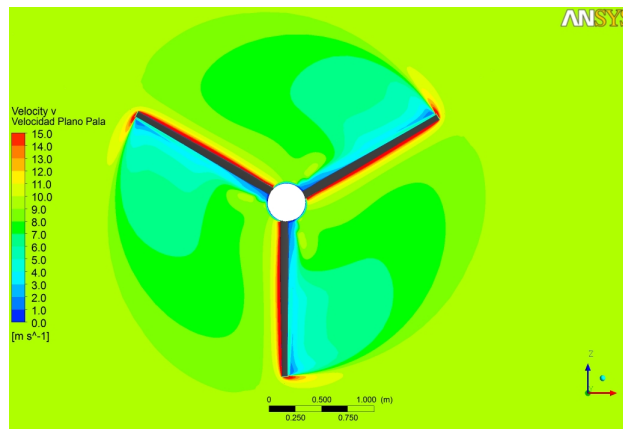


Figure 11: Velocity field at rotor plane.

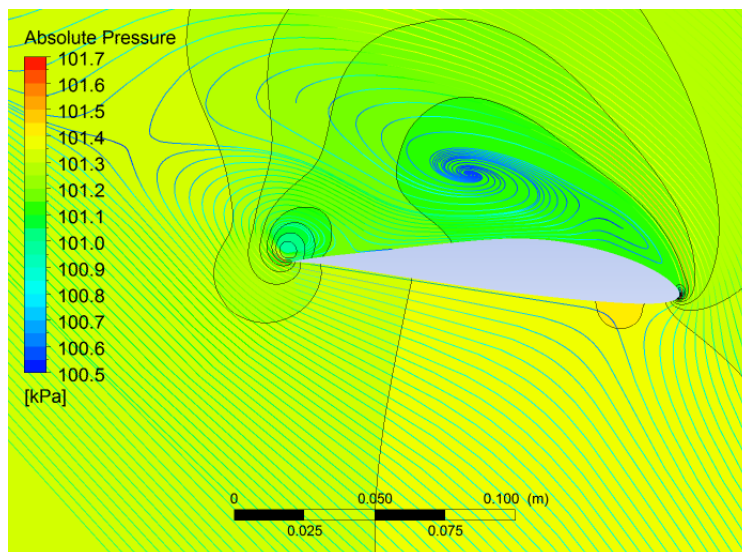


Figure 12: Pressure distribution at 200mm from the hub.

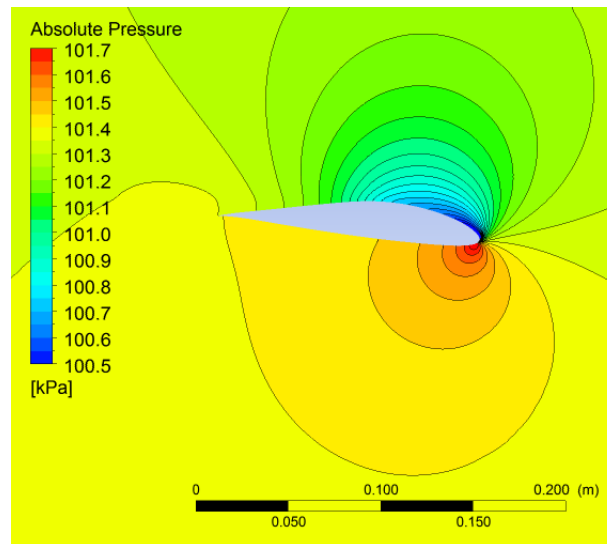


Figure 13: Pressure distribution at 800mm from the hub.

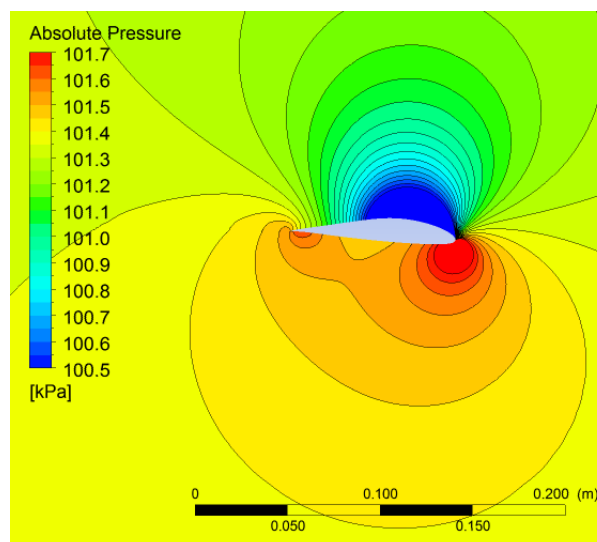


Figure 14: Pressure distribution at 1500mm from the hub.

3 CONCLUSIONS

Costa-I wind turbine aerodynamic characteristics were investigated by means of analytical and 2D and 3D CFD models. Developed models show good agreement with experimental results. In particular, turbine power output vs. wind speed curve has been predicted and good match between simulation results and power generation data retrieved from the field is observed.

Developed CFD models can be used to predict pressure distribution along the blades, and coupled with structural models, in order to perform FSI calculations. These calculations will be used in the future to perform structural optimization of the blades.

REFERENCES

- Althaus D. *Niedriggeschwindigkeitsprofile*. Friedr. Vieweg & Sohn Verlagsgesellschaft mbH, 1996.
- Betz A. *Windenergie und ihre Ausnutzung durch Windmühlen*. Ökobuch Verlag, 1994.
- Clausen P. and Wood D. Research and development issues for small wind turbines. *Renewable Energy*, 16:922–997, 1999.
- Cooper P., Kosasih P., and Ledo L. Roof mounting site analysis for micro-wind turbines. *Renewable Energy*, 36:1379–1391, 2010.
- de Vries O. *Fluid Dynamic Aspects of Wind Energy Conversion*. AGARD, 1979.
- Kaldellis J. Parametric investigation concerning dimensions of a stand-alone wind-power system. *Applied Energy*, 77:35–50, 2004.
- Manwell J., McGowan J., and Rogers A. *Wind energy explained*. Wiley, 2009.
- Peacock A., Jenkins D., Ahadzi M., Berry A., and Turan S. Micro wind turbines in the uk domestic sector, energy and buildings. *Renewable Energy*, 40:1324–1333, 2008.
- Pletcher R., Tannehill J., and Anderson D. *Computational Fluid Mechanics and Heat Transfer*. CRC Press, 2013.
- Ronit K., Singh M., and Rafiuddin A. Blade design and performance testing of a small wind turbine rotor for low wind speed applications. *Renewable Energy*, 50:812–819, 2013.